Spectrochimica Acta Part B 117 (2016) 23–28

Contents lists available at ScienceDirect

Spectrochimica Acta Part B

journal homepage: www.elsevier.com/locate/sab

Technical note

Determination of X-ray excitation spectra in micro X-ray fluorescence spectrometry with capillary optics

R.D. Perez [a,b,*], C. Sosa [b], V. Sbarato [c], J. Leani [b], H.J. Sánchez [a,b]

[a] FaMAF, Universidad Nacional de Córdoba, (5000) Ciudad Universitaria, Córdoba, Argentina
[b] IFEG-CONICET, Ciudad Universitaria, Córdoba, Argentina
[c] FCA, Universidad Nacional de Córdoba, (5000) Ciudad Universitaria, Córdoba, Argentina

ARTICLE INFO

Article history:
Received 6 October 2014
Accepted 21 December 2015
Available online 30 December 2015

Keywords:
Micro-XRF
Capillary optics
Calibration

ABSTRACT

The quantitative X-ray fluorescence microanalysis by fundamental parameters requires the knowledge of the energy distribution of the excitation beam. When this beam is produced by capillary optics, its high intensity and anisotropy complicate a direct determination. An alternative is an indirect determination based on measurement of induced X-ray fluorescence in a set of targets. In this work the X-ray excitation spectrum is determined by an iterative deconvolution process of the fundamental parameter expression for the X-ray fluorescence intensities. The method has the advantage that it does not require any assumption about the energy distribution of the X-ray source or the energy dependence of the lens transmission. Numerous XRF targets of pure elements with emission lines covering the full energy range of the X-ray source are employed. The only requirement on the targets is a high homogeneity in its composition. In fact, it does not impose any condition on the sample thickness. The accuracy observed in the validation process implemented with reference materials is similar to that reported with alternative approaches: 5% for main components, 10% for minor elements and 15% for trace elements.

1. Introduction

The X-ray fluorescence (XRF) from a bulk sample has a non-linear dependence with element concentrations because of the so called matrix effects which particularly affect the quantitative analysis by microanalysis of X-ray fluorescence (micro-XRF) [1,2]. A possibility to correct matrix effects consists in the comparison of the X-ray fluorescence emission with a set of standards of similar composition to that of the investigated object [3]. Another possibility consists in the application of the Fundamental Parameter model (FP) which requires few calibration standards for the quantification of a wide range of matrices [2,4]. This method was used in this work because of its versatility.

There exists a set of analytical equations in FP that describe the physical processes in the sample that lead to the emission of XRF. It requires a database of fundamental parameters, like photo ionization cross sections, fluorescence yields and transition probabilities; and also the spectral distribution of the excitation radiation. In case of polychromatic tube excitation combined with a capillary lens, the energy spectral distribution of the excitation radiation cannot be measured directly at the focal spot of the optical component because of the high flux in the output. One could increase the distance between the detector and the lens as to reduce the photon flux but since the photon flux is anisotropic, a partial determination of the excitation spectrum would be obtained. For all above, an indirect measurement of the energy spectral distribution of the excitation radiation is preferable. The methods available can be classified into two groups according to the measurements required: one group employs X-ray scattering [5,6] and the other induced X-ray fluorescence in targets [7–10]. All of them have been validated by means of elemental quantification of certified reference materials. The accuracy of these approaches has been estimated by comparing the similarity in concentrations with certified values. Some approaches adopt assumptions for the energy profile of the excitation spectrum which require a previous deduction from experimental means [8–10]. In the Rossinger approach [10], this energy profile is approximated by a suitable model function with free parameters. Its type is suggested by the assumed behaviour known from a spectrum of scattered primaries. If this previous step is solved, then the Rossinger approach becomes a possible alternative to determine the excitation spectrum for spectrometers with capillary optics.

The method by X-ray scattering employs light matrices to characterize the excitation spectrum. A good precision for high energy photons can be obtained because in this regimen multiple scattering effects on the target can be neglected. The reported accuracy of the approach proposed by Padilla et al. [6] is better than 15% for major and minor elements in homogeneous samples (glasses, ceramics).

One of the earliest methods using X-ray fluorescence induced in targets was developed by Delgado et al. [7]. It consists in the measurement of the X-ray fluorescence intensity for several thick targets as to cover the emission energy interval of the X-ray source. The method has the advantage that it does not require any assumption about the emission

* Corresponding author at: FaMAF, Universidad Nacional de Córdoba, Argentina.

http://dx.doi.org/10.1016/j.sab.2015.12.009
0584-8547/

spectrum of the X-ray source. The accuracy was tested in samples containing only two components and the reported accuracy was less than 10%. The accuracy can be improved by adding more XRF lines in the energy interval of the X-ray source. A drawback of this method is that the quantity obtained is the cumulative spectral distribution (which is the integral of the X-ray spectral distribution). It means that a reformulation of the quantification procedures is required in order to write the FP equations as a function of the cumulative spectral distribution.

A more recent methodology consists of the measurement of the Kα X-ray fluorescence intensity of several thin targets as to cover the emission energy interval of the X-ray source [8]. It obtains the transmission of the lens assuming an energy dependence of the transmission function and applying the second mean value theorem. In addition, this method requires the input of the X-ray tube spectrum, but to obtain it requires dismounting the lens at least one time for an experimental determination or the employment of a theoretical model. The reported accuracy of this method for major and minor elements is less than 10%.

In the present work this last methodology was expanded to obtain the excitation spectrum for micro-XRF including the two main advantages of Delgado's approach *i.e.* the employment of robust thick targets and the lack of assumptions on the physical characteristics of the X-ray source.The proposed approach is described in detail and applied to characterize the X-ray source of our laboratory. Validation by means of quantitative analysis of several standard materials is also shown.

2. Theoretical background

2.1. Micro-XRF intensity

In this work the geometry 45°–45° for micro-XRF was assumed for the theoretical descriptions since it was employed in the experimental measurements and is most usually implemented in micro-XRF spectrometers. Thus the incident beam and the detected beam form 90° between them and 45° with the sample. In addition the XRF targets were considered infinitely thick as to robustify the calibration approach. However the proposed approach is valid for any micro-XRF configuration,„ (e.g. other incident angles, emergent angles, or sample thickness). The fundamental parameter model applied to our micro-XRF setup gives rise to the following mathematical expression for the XRF photon flux of an element *i*:

$$N_i = \int_{E_{Bi}}^{E_{\max}} \frac{dN_0}{dE}(E) K(E_{Fi}, E) dE \tag{1}$$

where dN_0/dE is the energy distribution of the excitation beam and K is the kernel of the equation given by:

$$K(E_{Fi}, E) = \frac{\Delta\Omega}{4\pi}\, \epsilon(E_{Fi}) e^{-\mu_{air}\rho_{air}t} \frac{\sqrt{2}\, C_i a_i(E)}{(\mu(E_{Fi}) + \mu(E))}\, (1 + H_i) \tag{2}$$

$$\text{with } a_i(E) = \sigma_i(E)\omega_i p_i \left(1 - \frac{1}{j_i}\right).$$

The nomenclature used in the above equations is summarized in Table 1. In the particular case in which an X-ray tube is employed as the photon source, the spectral energy distribution is composed of a continuous curve produced by the bremsstrahlung effect, and several discrete lines which are the characteristic radiation lines of the anode material. For the sake of simplicity both parts of the spectrum will be determined separately.

2.2. Characteristic radiation

The discrete lines of the characteristic radiation produced by an X-ray tube can be indirectly determined analyzing the dispersion in a thin light matrix. Each of them produces two new lines in the scatter spectrum, one at the same energy by Rayleigh effect and other at slightly smaller energy by Compton effect. For a thin target of thickness d the FP model predicts similar descriptions for the intensity of both lines. If the photons of a characteristic line of energy E_L and intensity N_{0L} are scattered by one of the previous processes then the photon flux of the scattered beam can be written as:

$$N_{Ls} = S(E_{Ls}, E_L) N_{0L} \tag{3}$$

where E_{Ls} is the energy of the scattered line and S is a function similar than the kernel K given by:

$$S(E_{Ls}, E_L) = \frac{\Delta\Omega}{4\pi}\, \epsilon(E_{Ls}) e^{-\mu_{air}\rho_{air}t} \sqrt{2}\, \frac{d\sigma}{d\Omega}(E_L) \frac{\left[1 - \exp\left(-(\mu(E_{Ls}) + \mu(E_L))\sqrt{2}\, \varrho\, d\right)\right]}{(\mu(E_{Ls}) + \mu(E_L))}. \tag{4}$$

Here $d\sigma/d\Omega$ represents the differential cross section for coherent or incoherent scattering evaluated for a scattering angle of 90° according to the selected discrete line. In the particular case of the Rayleigh line the function S adopts a simpler form since $E_L = E_{Ls}$:

$$S(E_L, E_L) = \frac{\Delta\Omega}{4\pi}\, \epsilon(E_L) e^{-\mu_{air}\rho_{air}t} \sqrt{2}\, \frac{d\sigma}{d\Omega}(E_L) \frac{\left[1 - \exp\left(-2\sqrt{2}\mu(E_L)\, \varrho\, d\right)\right]}{2\mu(E_L)}. \tag{5}$$

Previous equations were derived assuming single scattering in the sample which means that the thickness d of the sample is small enough to neglect higher order interactions. Mathematically,

$$d \ll \frac{1}{\mu(E_L)}. \tag{6}$$

This means that the thickness d is much smaller than the mean free path of the radiation. From the Eq. (3), it is possible to calculate the photon flux for every characteristic line fitting the coherent and/or incoherent scattering lines and evaluating the S function. A specific Monte Carlo simulation program developed in FORTRAN language was employed for a precise evaluation of the S function. It requires the input of the excitation beam cross section, the thickness of the sample, its composition, the distance sample-detector, and the dimensions of the detector collimator.

2.3. Continuous spectrum

The FP model allows calculating the contribution N_{ci} of the continuous part of the excitation spectrum to the XRF photon flux of an element

Table 1
Definition of the parameters employed in Section 2.

N_i	XRF photon flux emitted by element *i*.
E_{Bi}	Absorption edge for XRF emission of element *i*.
E_{max}	Maximum energy of the excitation spectrum.
E_{Fi}	Energy of the XRF emission of element *i*.
$dN_0/dE(E)$	Energy distribution at energy E of the excitation spectrum.
$\Delta\Omega$	Solid angle subtended by the detector.
$\varepsilon(E)$	Detector efficiency at energy E.
μ_{air}	Mass attenuation coefficient for air at energy E_{Fi}.
ρ_{air}	Mass density of air.
t	Path length in air of the detected photon beam.
C_i	Mass fraction of element *i* in the sample.
$\sigma_i(E)$	Mass photoelectric coefficient of element *i* at energy E.
ω_i	Fluorescence yield for the excited shell of element *i*.
p_i	Line fraction of the element *i*.
j_i	Jump ratio for the excited shell of element *i*.
$\mu(E)$	Mass attenuation coefficient of the sample at energy E.
H_i	Contribution of the secondary excitation on the XRF emission of element *i*.

i by means of the subtraction of the characteristic radiation contribution to N_i:

$$N_{ci} = N_i - \sum_j P(E_{Lj} - E_{Bi}) K(E_{Fi}, E_{Lj}) N_{0Lj}. \quad (7)$$

Here $P(E)$ is a step function equal to 1 for energies higher than zero, and zero otherwise, and the sum covers all the characteristics lines E_{Lj} of the excitation spectrum. In this section it is assumed that the characteristic lines of the excitation spectrum were already determined following the procedure described above. The continuous part of the excitation spectrum dN_{c0}/dE appears in the following analytic expression for N_{ci}:

$$N_{ci} = \int_{E_{Bi}}^{E_{max}} \frac{dN_{c0}}{dE}(E) K(E_{Fi}, E) dE. \quad (8)$$

The proposed approach to obtain dN_{c0}/dE uses the second mean value theorem for integrals to evaluate the continuous part of the excitation spectrum in an energy E_{mi} placed between the integration limits. This theorem establishes that for a continuous function f and an integrable, positive function g there exist a number x_m such that:

$$\int_a^b f(x) g(x) dx = f(x_m) \int_a^b g(x) dx \quad (9)$$

with $a < xm < b$. The number $f(xm)$ is called the g-weighted average of f on the interval $[a,b]$. In this context f represents dN_{c0}/dE and g the kernel of the Eq. (1). The weighted mean energy can be obtained by fitting E_{mi} in the previous equation, which requires an estimation for the energy dependence of dN_{c0}/dE. In the present approach, the XRF intensities of several targets covering the emission energy interval of the X-ray source are employed to deduce the energy dependence of dN_{c0}/dE. The XRF targets are ordered with absorption edges gradually decreasing to implement an inductive process. Instead of applying the second mean value theorem in the full interval $[E_{Bi}, E_{max}]$, it is applied in the restricted interval $[E_{Bi}, E_{Bj}]$ with $j < i$ as to reduce the uncertainty in Emi. Thus, the first interval in the inductive process is $[E_{B1}, E_{max}]$, where the application of the second mean value theorem allows obtaining $dN_{c0}/dE(E_{m1})$ from the following equation:

$$\int_{E_{B1}}^{E_{max}} \frac{dN_{c0}}{dE}(E) K(E_{F1}, E) dE = \frac{dN_{c0}}{dE}(E_{m1}) \int_{E_{B1}}^{E_{max}} K(E_{F1}, E) dE. \quad (10)$$

The integral in the left hand side is obtained by measuring N_1 and the integral in the right hand side is calculated by FP. To calculate E_{m1}, a linear energy dependence is assumed for dN_{c0}/dE in the interval $[E_{B1}, E_{max}]$ (which is zero at E_{max}). The result of the analysis is an experimental point $(E_{m1}, dN_{c0}/dE(E_{m1}))$. For a subsequent XRF target i, the application of the second mean value theorem at the interval $[E_{Bi}, E_{Bj}]$ gives $dN_{c0}/dE(E_{mi})$ from a similar equation than the previous one:

$$\int_{E_{Bi}}^{E_{Bj}} \frac{dN_{c0}}{dE}(E) K(E_{Fi}, E) dE = \frac{dN_{c0}}{dE}(E_{mi}) \int_{E_{Bi}}^{E_{Bj}} K(E_{Fi}, E) dE. \quad (11)$$

Here the integral of the right hand side is obtained as before. The left hand side of the equation, defined as N_{cij}, can be obtained by subtracting to N_{ci} the contribution of the continuous excitation spectrum from energies higher than E_{Bj}. This contribution can be calculated by employing the results of the previous step in this inductive process. Mathematically the formulae for N_{cij} is the following:

$$N_{cij} = \int_{E_{Bi}}^{E_{Bj}} \frac{dN_{c0}}{dE}(E) K(E_{Fi}, E) dE = N_{ci} - \int_{E_{Bj}}^{E_{max}} \frac{dN_{c0}}{dE}(E) K(E_{Fi}, E) dE. \quad (12)$$

To obtain E_{mi}, dN_{c0}/dE is fitted in the interval $[E_{Bi}, E_{max}]$ by a derivable elementary function. At this step, the set of experimental points $(E_{mk}, dN_{c0}/dE(E_{mk}))$ with k from 1 to $(i - 1)$ have been already determined in our inductive process. For the last point $(E_{mi}, dN_{c0}/dE(E_{mi}))$, E_{mi} is selected from a discrete set of uniformly distributed values in the interval $[E_{Bi}, E_{Bj}]$. At each selected energy, a polynomial function of order $(i - 1)$ is fitted by least squares to all experimental points $(E_{mj}, dN_{c0}/dE(E_{mj}))$ and then the difference of both sides of the previous equation is evaluated. The result for E_{mi} is the value that minimizes the difference.

The inductive process presented could require several polynomial fittings since a new polynomial function is employed every time that E_{mi} is changed. To reduce the number of steps a small interval $[E_{Bi}, E_{Bj}]$ is conveniently chosen as to limit the possible values for E_{mi}. This can be done by employing a high number of XRF targets. However, if dN_{c0}/dE is a decreasing function, a small interval $[E_{Bi}, E_{Bj}]$ may not be necessary. For these cases there is not any problem because E_{mi} will be close to E_{Bi} – even for wider intervals $[E_{Bi}, E_{Bj}]$ – since the kernel is also a decreasing function with energy for all elements (see Fig. 1). A special advantageous case is observed for very thin standards where the kernel is a fast decreasing function, which always maintains E_{mi} close to E_{Bi} even for the full interval $[E_{Bi}, E_{max}]$ regardless the behaviour of dN_{c0}/dE [8]. In spite that choosing a small interval $[E_{Bi}, E_{Bj}]$ is preferred for searching E_{mi}, this selection produces instabilities in the calculation of E_{mi} when N_{cij} becomes comparable to its uncertainty. It was observed that values for N_{cij} in the order of 15% of N_{ci} avoid instabilities, which in the set of XRF targets used in this work was satisfied choosing $j = (i - 2)$. When the inductive process presents instabilities in one step, the uncertainty of the spectrum determination increases in the energy interval related to this step. In addition, the uncertainty propagates through the following steps of the inductive process according to Eq. (12). As a consequence, the lower energy part of the spectrum becomes more imprecise, which increases the uncertainty in the quantification of light elements by FP model.

The proposed iterative process is inspired in the Delgado's approach originally developed to obtain the cumulative spectral distribution of the excitation spectrum [7]. An important difference is that Delgado's approach uses a piecewise linear function to fit the experimental points, but here a least-square polynomial fit was employed for better accuracy. Effectively, this fit selects the curve that minimizes the uncertainties of the experimental points, which reduces the instabilities of the global calculation. The election of a polynomial function is supported by the approximation theory of Taylor series. It is important to highlight that the degree of the polynomial function must be lower than the number of fitting points for an appropriate application of the regression analysis. In spite that a polynomial fitting function is suggested by the authors, the least squares fit can be implemented with another type of approximate functions with similar convergence.

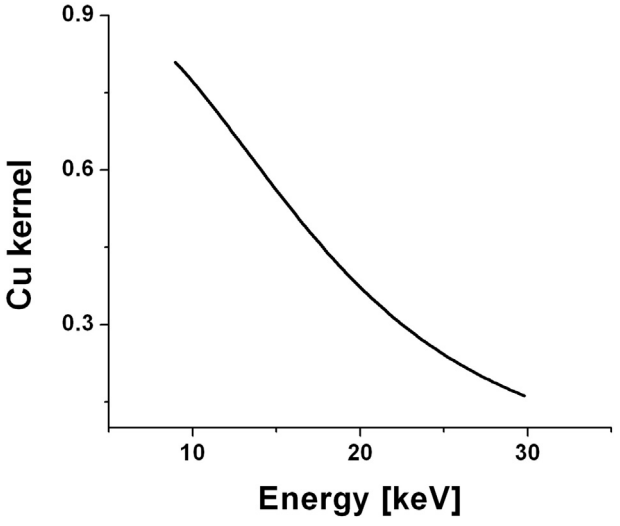

Fig. 1. Energy dependence of the kernel for copper XRF emission, calculated in a pure copper matrix. This fast decreasing behavior is typical for the kernel of pure elements.

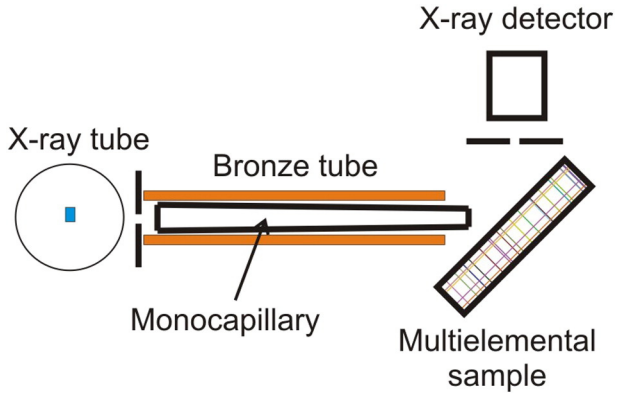

Fig. 2. Schematic diagram of the experimental setup employed to determine the polychromatic excitation spectrum by means of the proposed approach.

The proposed fitting process smoothens the jumps of the excitation spectrum that are produced by the absorption edges of the anode material. This could affect the element quantification with absorption edges close but lower than the jumps. However, these elements usually are analyzed changing the X-ray tube to avoid the overlapping of the XRF emissions with the characteristic lines of the anode material. For this reason, the approximation can be considered accurate for elemental quantification by micro-XRF but their effects should be evaluated for other possible applications.

3. Materials and method

3.1. Instrumentation

The high power X-ray source available in our laboratory is a Mo X-ray tube (Philips model PW2275/20). The Mo anode was in the horizontal plane with a focus dimension of 0.4 mm × 12 mm (long fine focus) but it was oriented as to obtain a point source. The lens axis was selected as the direction of maximum intensity of the X-ray beam, which was pointed down at 6° from the horizontal plane. This selection was made because it optimizes the input photon flux on the lens. In this way the X-ray source looks as a point source of 0.4 mm × 1.26 mm area. The maximum power supply of the X-ray generator was 3 kW.

The lens was mounted on a precision manually-controlled four-axis stage – up–down, left–right, and horizontal and vertical rotation – (*Newport* model Cat.LP-05A). It allows precise repeatability on the linear movements, with a resolution of 0.6 microns, and on the rotations, with an angular resolution of 1 mrad.

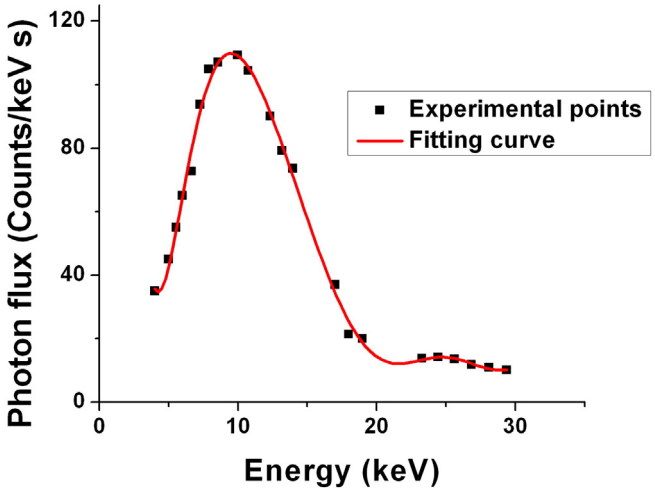

Fig. 3. Continuous part of the excitation spectrum determined by the proposed approach. A strong modulation of the bremsstrahlung profile by the capillary optic is observed, which accounts for the increase in the photon flux at low energies.

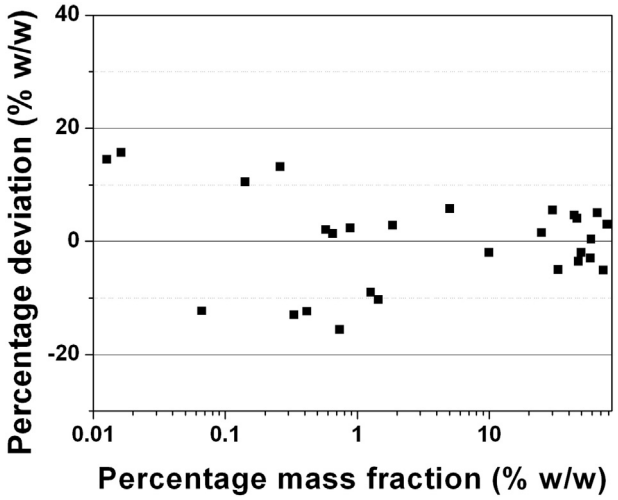

Fig. 4. Percentage relative error of the calculated mass fractions vs. certified values. For the mass fraction determinations, the reference standard samples described in Table 4 were analyzed by micro-XRF. The FP model derived from the proposed approach was applied for these quantifications.

The parameters of the monocapillary employed in this work are listed in Table 2. It was made of borosilicate glass and has a high quality conical inner profile. The wall of the lens is very thick for an effective attenuation of the high energy X-ray photons.

A motorized sample holder controlled by a computer helps the repeatability of the measurements. It uses *Rexroth* ball bearing screws to guarantee a spatial resolution of 13 microns for the three orthogonal directions. XRF emission was collected by a Si-PIN detector (*Moxtek* XPIN-XT), an ORTEC amplifier (model A590), and AMPTEK MCA (model 8000D). The X-ray detector was positioned perpendicular to the excitation beam along the horizontal plane. The distance from the entrance window of the detector and the surface sample was 12 mm. The detector efficiency was determined by a Monte Carlo simulation using the software PENELOPE [11] with input data provided by *Moxtek*. A schematic diagram of the employed setup is shown in Fig. 2.

The proposed calibration approach was implemented in our laboratory employing a standard block containing 44 pure elements, placed in a metal disk of 32 mm diameter (Micro-Analysis Consultants Ltd.). The accuracy of the approach was tested employing a similar block containing 53 mineral reference materials (MAC-Micro-Analysis Consultants Ltd.), and two multielemental reference material glass beads: a Breitlander bead (code RM-BRE2) with 30 elements, and a BAM bead (Federal Institute for Materials Research and Testing-Germany, code BAM S005A) with 28 elements.

3.2. Excitation spectrum determination

The micro-XRF spectrometer of our laboratory was operated at 30 kV and 20 mA. The analyzed elements from the block standard with pure elements were those with Kα or Lα XRF lines in the energy range of the excitation spectrum. The Kα and Lα XRF lines were selected because they have high intensity, and their mathematical expression (from FP model) requires only one absorption edge (which is not the

Table 2
Description of the lens employed in this work. L is the length of the lens, D_i is the external input diameter d_i is the inner input diameter, D_f is the external output diameter, d_f is the inner output diameter and α is the tilt angle.

L	D_i	d_i	D_f	d_f	A
80.3 mm	5.2 mm	0.77 mm	2.7 mm	0.040 mm	4.5 mrad

case for other XRF lines as for example Lβ). The list of elements analyzed, with some of their relevant properties, is shown in Table 3. Every element was analyzed using the Kα line except Pb in which it was used the Lα line for XRF measurements. The acquisition time for all elements was 300 s except for Ag, Cd and In in which it was 600 s since the registered counting rates for these elements were too low. The XRF intensities were obtained using the AXIL software [12].

The characteristics lines (Kα and Kβ) of the Mo X-ray tube were measured by the X-ray scattering from a high purity PMMA thin foil of 0.5 mm thickness. The mean free path for Mo-Kα and Mo-Kβ are 7.6 mm and 14.7 mm, respectively, which justify to neglect every other high order contribution to the X-ray scattering.

4. Results and discussions

4.1. Excitation spectrum determination

The energy distribution for the continuous part of the excitation spectrum of our micro-XRF spectrometer obtained by the proposed approach is shown in Fig. 3. The weighted mean energies E_{mi} are included in Table 3. In addition, this table contains the differences between the XRF photon fluxes measured and calculated with Eq. (1). They show the low dispersion of the experimental points which is a good indicator of the accuracy of the proposed approach. For the *K* lines of the excitation spectrum, the obtained relation $K\alpha/K\beta$ was 3.145 which is quite smaller than the theoretical value 5.181 for isolated Mo atoms [13]. Selfabsorption of the X-ray lines in the anode is the main cause of this strong discrepancy. To give an idea of the *K* line intensities, they were compared with the contribution from the continuos part in the energy interval from 17 to 30 keV. The ratio between this portion of the continuos part and the sum of the intensities for both characteristics lines was 0.683.

The calculations required by the proposed approach consist in two parts. The first part evaluates the intensities of the characteristic lines by fitting with the data obtained from the X-ray scattering of a PMMA thin foil. The theoretical fitting model previously described in Section 2 uses the differential cross sections for coherent and incoherent scattering tabulated by Hubbel et al. [14], and the mass photoelectric and attenuation coefficients from McMaster et al. [15]. The Monte Carlo simulation code written in FORTRAN language carefully considers all possible trajectories for the single scattered X-ray photons in order to obtain the *S* scattering function described in Eq. (3). The second part of the calculations is related to the determination of the continuous part of the excitation spectrum. A specific code in Octave 3.6.2 was written to fit the measured XRF intensities with the FP model. It employs the mass photoelectric and attenuation coefficients from McMaster et al. [15], adopted values for fluorescence yields from Krause [16] and fraction lines from Clark [13]. The indirect ionization in the L_3 subshell of lead created by Coster–Kronig effects was taken into account in the calculations employing Krause's probabilities [16].

Table 3
List of the pure elements from the MAC standard block used to obtain the continuous part of the excitation spectrum. From left to right the columns have the following information for each element: name, atomic number Z_i, iteration number *i*, mean energy of XRF line E_{Fi}, absorption edge E_{Bi} and weighted mean energy E_{mi} for the interval [E_{Bi}, E_{Bi-2}]. The last column shows the relative differences between the XRF photon fluxes measured and calculated with Eq. (1) by means of the fitted excitation spectrum.

Element	Z_i	*i*	E_{Fi} (keV)	E_{Bi} (keV)	E_{mi} (keV)	%RD
Sc	21	24	4.088	4.489	4.950	5%
Ti	22	23	4.508	4.963	5.450	4%
V	23	22	4.948	5.462	5.893	3%
Cr	24	21	5.411	5.987	6.357	2%
Mn	25	20	5.895	6.535	7.264	3%
Fe	26	19	6.400	7.109	7.901	3%
Co	27	18	6.925	7.707	8.566	2%
Ni	28	17	7.472	8.329	9.978	4%
Cu	29	16	8.041	8.978	10.734	2%
Zn	30	15	8.631	9.657	11.330	3%
Ge	32	14	9.876	11.100	13.180	2%
As	33	13	10.532	11.860	13.963	3%
Se	34	12	11.210	12.649	15.012	4%
Pb	82	11	10.542	13.041	15.671	5%
Sr	38	10	14.142	16.101	16.566	2%
Y	39	9	14.933	17.032	17.440	2%
Zr	40	8	15.746	17.993	17.993	2%
Nb	41	7	16.584	18.981	18.981	2%
Ru	44	6	19.234	22.112	23.276	1%
Rh	45	5	20.167	23.217	24.439	2%
Pd	46	4	21.122	24.341	25.622	1%
Ag	47	3	22.103	25.509	26.852	2%
Cd	48	2	23.108	26.704	28.109	3%
In	49	1	24.137	27.920	29.389	4%

4.2. Quantification of reference standard samples

To validate the calibration result, the obtained excitation beam spectrum was used for the quantification of micro-XRF measurements of standard samples by FP. The XRF intensities were obtained fitting Voight profiles to the XRF lines of the spectra with Axil software [1]. The FP calculations were carried out by a self written software code which includes secondary fluorescence contributions. Each sample was measured in three different points as to check homogeneity. The arithmetic mean value for XRF intensities was taken as the best estimate of the standard XRF intensities. From the 53 mineral standard block, ten samples were measured since they were the only ones with the emission XRF lines in the calibrated range, and without serious line overlappings (otherwise the peak fitting process introduces high dispersion in the results). The reference samples are listed in Table 4. In the case of the glass analysis, the mass fraction of oxygen was calculated assuming the oxidation states given in the certificates. The dark matrix was assumed as known, taking light element concentrations from the certificates.

The percentage relative error of the calculated concentrations is plotted as a function of the certified values in Fig. 4. As expected, the quality of the quantitative analysis depends on the absolute amount of the analyte in the sample. Most of the calculated values fit the certified data within a range of ±5% for mass percentages of more than 1%. For mass percentages between 0.1% and 1% the calculated mass fractions do not vary from the certificate by more than 10%. For elements with lower mass percentages the values are within a range of 15%.

The small relative deviations in the quantification obtained with the proposed calibration approach confirm its accuracy. It agrees with the low dispersion observed in the fitted experimental points of the continuous part of the excitation spectrum. It is important to highlight that the results have been obtained without any assumption about the energy profile of the excitation spectrum. Then, the proposed approach could be useful in those cases when the transmission of the optical component is unknown, as is in the case of capillary optics. A drawback is that it requires a numerous set of certified concentrations with XRF lines as to cover the energy region of the excitation spectrum. It implies that more effort for measurements and data processing is needed, comparing to previous approaches which employ a semi-empirical function to fit the excitation spectrum [9,10]. Therefore, it is recommended only when the excitation spectrum profile is unknown as is in the case of micro-XRF spectrometers with capillary optics. A highlight of the proposed approach is that the only requirements on the standards is high homogeneity in their composition. Therefore, the set of standards can be collected from a wide variety of configurations including infinitely thick samples as well as foils or thin films.

5. Conclusions

In the present work a new approach for calibration of micro-XRF spectrometers has been developed and validated. It requires a set of homogeneous standards with XRF lines as to cover the energy range of the

Table 4
Description of the reference standard samples employed to validate the proposed approach. The elements of the standard samples analyzed in this process are listed in the last column. It also includes in brackets the certified mass fraction (percentage) for each element.

Name	Producer	Type	Analyzed elements
E2	Breitlander	Multielemental glass	Mn (5.0%), Co (0.58%), Ni (1.45%), Cu (0.66%), Zn (0.74%), As (0.33%), Sr (0.26%), Y (0.14%).
S005A	BAM	Multielemental glass	Zn (0.0163%), Sr (0.0128%), Zr (0.0665%).
Iodargyrite (AgI)	MAC	Natural mineral	Ag (46.49%)
Willemite (Zn_2SiO_4)	MAC	Natural mineral	Zn (58.34%)
Pentlandite ($(FeNi)_9S_8$)	MAC	Natural mineral	Fe (30.22%), Ni (33.41%)
Bustamite ($(Mn,Ca)SiO_3$)	MAC	Natural mineral	Ca (10.61%), Mn (25.04%)
Rutile (TiO_2)	MAC	Natural mineral	Fe (0.89%), Ti (59.26%)
Nickeline (NiAs)	MAC	Natural mineral	Co (1.86%), Ni (49.88%), As (47.41%)
Magnetite (Fe_3O_4)	MAC	Natural mineral	Fe (73.41%)
Pirite (FeS_2)	MAC	Natural mineral	Fe (44.08%)
Zircon ($ZrSiO_4$)	MAC	Natural mineral	Zr (51.83%), Hf (1.08%)
Cassiterite (SnO_2)	MAC	Natural mineral	Sn (78.77%)
Gallium phosphide (GaP)	MAC	Natural mineral	Ga (69.24%)

X-ray source. The proposed approach admits thick standards with higher mechanical resistance and durability than foils or thin films. An iterative deconvolution process of the FP expression for the XRF intensities is employed, which expands a previous proposal of Wolff et al. [8], and is inspired in the work of Delgado [7]. It does not rely on any assumption of the energy dependence of the lens transmission so the approach should be valid for any kind of optics. For this reason, it is recommended to use this method when the energy profile of the focalization lens is unknown (as in the case of capillary optics). The result of the proposed approach is the determination of the excitation spectrum energy distribution which can be helpful for qualitative and quantitative analysis by micro-XRF. The accuracy observed in the validation process is similar to that reported with alternative approaches [6–8].

Acknowledgment

Part of the work was carried within the framework of a Coordinated Research Project of the International Atomic energy Agency (RC-16762). Others institution involved are CONICET and MINCyT.

References

[1] J. Sherman, The theoretical derivation of fluorescent X-ray intensities from mixtures, Spectrochim. Acta Part B 7 (1955) 283–306.
2 T. Shiraiwa, N. Fujino, Theoretical calculation of fluorescent X-ray intensities in fluorescent X-ray spectrochemical analysis, Jpn. J. Appl. Phys. 5 (1966) 886–899.
3 A.J. Klimasara, Mathematical modelling of XRF matrix correction algorithms with an electronic spread-sheet, Adv. X-ray Anal. 37 (1994) 647–656.
4 J. Criss, L. Birks, Calculation methods for fluorescent X-ray spectrometry. Empirical coefficients versus fundamental parameters, Anal. Chem. 40 (1968) 1080–1086.
5 W.T. Elam, J.A. Nicolosi, R.B Shen, B.E. Scruggs, Scatter spectra method for X-ray fluorescent analysis with optical components. US Patent 6845147B2 (2005).
6 P. Padilla, P. Van Espen, A. Abrahantes, K. Janssens, Semiempirical approach for standardless calibration in micro-XRF spectrometry using capillary lenses, X-Ray Spectrom. 34 (2005) 19–27.
7 V. Delgado, Indirect method for the determination of X-ray tube primary spectra: application to X-ray fluorescence analysis, X-Ray Spectrom. 31 (2002) 353–357.
8 T. Wolff, W. Malzer, I. Mantouvalou, O. Hahn, B. Kanngiesser, A new fundamental parameter based calibration procedure for micro X-ray fluorescence spectrometers, Spectrochim. Acta Part B 66 (2011) 170–178.
9 R. Mainardi, R. Barrea, Indirect method of X-ray spectra determination by XRF, X-Ray Spectrom. 25 (1986) 190–195.
10 V. Rössiger, Quantitative XRF analysis of surface layers: influence of primary energy distribution and enhancement, X-Ray Spectrom. 17 (1988) 107–115.
11 F.Salvat, J.M. Fernandez-Varea, E.Acosta and J.Sempau: "PENELOPE, A Code System for Monte Carlo Simulation of Electron and Photon Transport", Proceedings of a Workshop/Training Course, OECD/NEA 5–7 November 2001 NEA/NSC/DOC(2001)19. ISBN:92-64-18475-9.
12 P.M. Van Dyck, R. Van Grieken, Absorption correction via scattered radiation in energy-dispersive X-ray fluorescence analysis for samples of variable composition and thickness, Anal. Chem. 52 (1980) 1859–1864.
13 A.A. Markowicz, Chapter 1 X-ray Physics, in: R. Van Grieken, A.A. Markowicz (Eds.), Handbook of X-ray Spectrometry, 2nd ednMarcel Dekker, New York 2002, pp. 1–74.
14 J.H. Hubbell, V.J. Veigele, E.A. Briggs, R.T. Brown, D.T. Cromer, R.J. Howerton, Atomic form factors, incoherent scattering functions, and photon scattering cross sections, J. Phys. Chem. Ref. Data 4 (3) (1975) 471–538.
15 W.H. McMaster, N. Kerr Del Grande, J.H. Mallett, J.H. Hubbell, Compilation of X-ray Cross Sections, Lawrence Radiation Laboratory (Livermore) Report UCRL-50174, Sec. II, Rev. 1, University of California, 1969.
16 M.O. Krause, Atomic radiative and radiationless yields for K and L shells, J. Phys. Chem. Ref. Data 8 (2) (1979) 307–327.